



An investigation into electron isolation efficiencies and scale factors in the ATLAS detector

William Coulton, University of Oxford, UK

September 6, 2012

Abstract

This analysis explores the scale factors and efficiencies associated with three types of electron isolation cut. These cuts were used for analysis of the electron positron decay mode of the Z boson in the Atlas detector. The tag and probe method was implemented to measure the efficiencies and from these the isolation scale factors were computed. The scale factors were computed separately for the complete 2011 Atlas data set (which has an integrated luminosity of $\int L(t) dt = 4.75 fb^{-1}$) and on the periods A and B data sets from 2012 (which have a total integrated luminosity of $\int L(t) dt = 6.05 fb^{-1}$). The scale factors' and efficiencies' dependency on pseudo-rapidity (η), the number of primary vertices (NumVtx) and mu (μ , a measure of the number of events per bunch collision) was investigated. The systematic error in the scale factors arising from our invariant mass range cut was calculated and found to be less than 0.2%. The study observed a mass dependence in both the efficiencies and in the scale factors and provides evidence suggesting this is a result of bremsstrahlung.

Contents

| | | |
|----------|--|-----------|
| 1 | Introduction | 3 |
| 2 | Data and Simulation | 4 |
| 2.1 | The Atlas Experiment | 4 |
| 2.2 | Monte Carlo Simulation | 5 |
| 2.3 | The Data Set | 6 |
| 3 | The Analysis Procedure | 6 |
| 3.1 | The Tag and Probe Method | 6 |
| 3.2 | Isolation Cuts | 7 |
| 3.3 | Scale Factor dependencies | 8 |
| 4 | Results and Analysis | 9 |
| 4.1 | Efficiency Cross Check | 9 |
| 4.2 | The pseudo-rapidity dependence of the efficiencies and scale factors . . . | 10 |
| 4.3 | Systematic Errors from the Mass selection | 12 |
| 4.4 | Mass Dependence | 13 |
| 4.5 | The Dependence on the Number of Primary Vertices | 15 |
| 4.6 | Mu Dependence | 17 |
| 5 | Conclusion | 19 |

1 Introduction

The Large Hadron Collider (LHC) at CERN, Geneva, is well known as the latest machine searching for the Higgs Boson, however this is not its only function. The data collected at the experiment halls in the LHC is very useful for studying the properties of the fundamental particles and for gaining insight into the fundamental forces (for example the data can be used to test our Quantum Chromodynamic (QCD) models). The LHC is a proton-proton collider which operated with a centre of mass energy $\sqrt{s} = 7$ TeV in 2010 and 2011, and $\sqrt{s} = 8$ TeV in 2012.

The LHC has four main experiments ATLAS, CMS, LHCb and ALICE. LHCb is an experiment which studies b quark physics with the aim of improving our understanding of CP violation and the matter-antimatter asymmetry. ALICE is an experiment which studies lead-lead nuclei collisions (the LHC also has runs during which it accelerates lead nuclei instead of protons) and analyses the resulting hot quark-gluon plasma. ATLAS and CMS are general detectors designed to study physics at high energies with the hope of constraining our models whilst also searching for new particles. The data used in this report was collected by the ATLAS detector (which will be discussed in more detail in 2.1) during 2011 and 2012.

This study focuses on the decay of the Z boson to an electron positron pair. Studying the Z boson is of interest not only because it provides valuable information about its properties, but can also because it helps improve the understanding of many fundamental process. The Z boson is useful for improving our understand of the electroweak force; this is done through studies of branching ratios and by comparisons with W^\pm bosons. At the LHC the Z boson is produced through the Drell- Yan process. By calculating this process' cross section from Z boson studies we can test QCD and also constrain parton distribution functions [1]. Finally an important decay of the Higgs boson is to ZZ and thus by studying Z bosons we can search for the Higgs boson.

The electron-positron decay mode is particularly useful as it provides a clean signal which is easily reconstructed and has backgrounds which are small and easy to calculate. The Z boson is also useful as it is frequently created and thus we have small statistical errors. For the properties of the Z boson to be accurately measured we must accurately measure the properties of the electrons and positrons and reduce the sources of error, such as signal contamination from the background..

This report presents part of the analysis procedure associated with reconstructing these electrons. To reduce contamination a set of cuts are applied to the electron-positron candidates. These cuts act on a variety of different properties of both the electrons, the Z boson candidates and the detector. This study investigated the effect of using different types of isolation cut and calculates corrections for the Monte Carlo data. The study investigated the isolation cut scale factors with a slight focus on the pile up dependency.

2 Data and Simulation

2.1 The Atlas Experiment

The ATLAS detector [2] is a barrel detector designed so that it can measure particles almost regardless of their direction. The detector is made up of several layers as is shown in figure 1. The innermost layer is made of tracking detectors and is surrounded by a superconducting solenoid which immerses the trackers in 2T magnetic field. There are three types of tracking detector the silicon pixel detector, the silicon strip detector (which together form the Semi-Conductor Tracker) and the Transition Radiation Tracker. These detectors detect the location of charged particles as they pass through (thus they are unable to detect neutral particles). From the signals deposited in each tracking layer it is possible to reconstruct the particles' paths, which will be curved due to the applied magnetic field. From the direction and magnitude of the curvature of the path we can gain information about the momentum and charge of the particle. In addition through searching for the presence of secondary or tertiary vertices we can gain information about the type of particle.

The next layer of detectors is the calorimeters, which are located just outside of the solenoid. There are two main types of calorimeter - the electromagnetic (EM) and the hadronic calorimeters- whose purpose is to measure the energy of the particles. These detectors work via periodic sampling; this means that they absorb energy in a heavy metal and then periodical measure the resulting shower properties and from this infer the energy of the particles. The EM calorimeter measures the energy of charged particles (eg electrons) and photons. It is a liquid argon calorimeter which has a high energy resolution and also good spatial resolution. The hadronic calorimeter detects particles which interact via the strong force, this detector has poorer resolution but can detect neutral hadrons in addition to charged particles.

The final layer is the muon detector. This part of the detector is contained within a toroidal magnet which creates a magnetic field of 2-8 T. The muon detectors are very large so that they can accurately measure the momentum of the muons. This is necessary to attain the highest event reconstruction efficiency we must measure the energy and momentum of all the particles as accurately as possible.

In addition to these layers in the barrel there is also some detectors on the end of the barrel, known as the end-cap detectors. These were designed to measure the properties of particles which travel relatively close to the beam line. There are calorimeters and muon detectors in the end-cap, but these are of lower resolution to those in the barrel.

At each event large numbers of particles are produced and measured resulting in the production of a large amount of information. It is impossible to store and process all the data produced by each event and thus we must apply some cuts. These cuts are implemented by the triggering system, which consists of three levels that are carefully

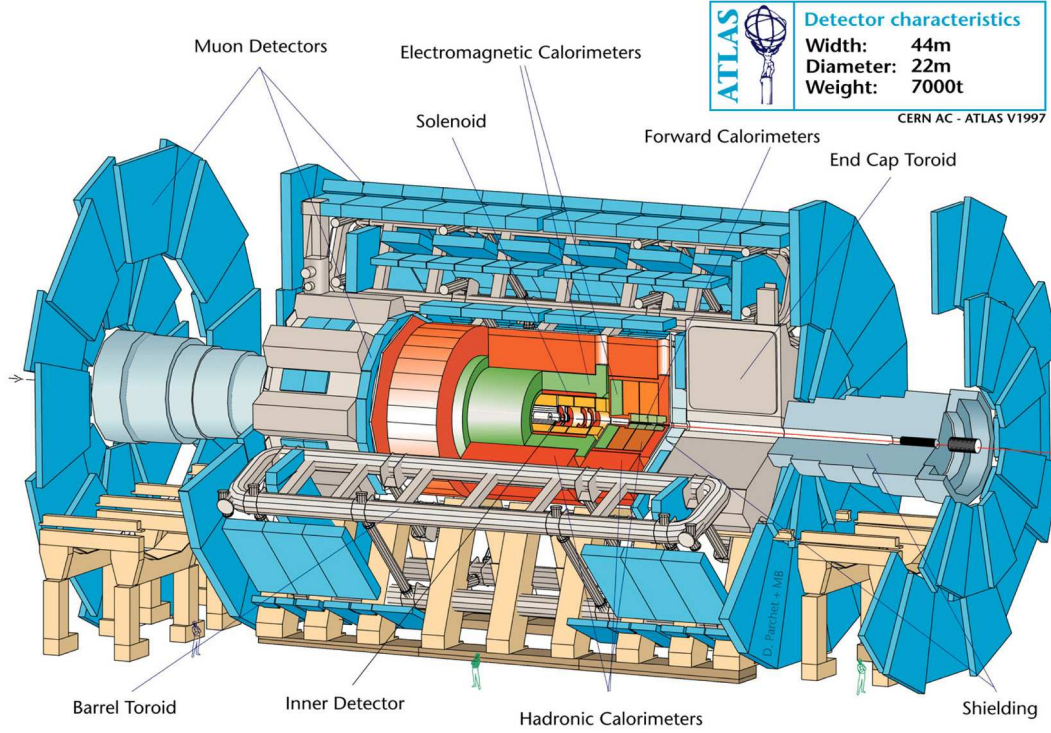


Figure 1: A schematic of the ATLAS detector

configured so that we retain useful data without introducing any bias. The triggers cut on a variety of parameters including the transverse momentum (p_T) and the pseudo-rapidity η (where $\eta = -\ln \tan \theta/2$).

The first level trigger is hardware-based; it was designed to be very quick and apply only crude cuts to remove objects that we definitely do not want; in this case it selects particles which may have high transverse momentum. It does not use the full granularity of the detector as it needs to be very quick. The higher level triggers use the full granularity of the detector and are much tighter cuts. The triggering process reduces the event rate by more than four orders of magnitude and so plays a vital role. The resulting data is subsequently preprocessed before being used in this analysis. The pre-processing uses the egamma stream; this stream contains events which have passed at least one electron or photon trigger.

2.2 Monte Carlo Simulation

To fully reconstruct an event, it is crucial to understand how the particles behave as they pass through the detector material and how the detector will respond to this stimulus. To test our understanding one has to use Monte Carlo (MC) simulations to randomly

generate events with a distribution dictated by theory. By comparing the Monte Carlo results with the actual data it is possible to judge the accuracy of the simulation and test our understanding of both the particles' and the detector's behaviour. The Monte Carlo simulations used in this report were generated using the PYTHIA [3] and PowHeg [4] programs. Often there are aspects of the experiment which cannot be accurately reproduced in the Monte Carlo and these effects are corrected for with the use of scale factors.

2.3 The Data Set

Two data sets were used in this analysis; the full 2011 data set and periods A and B of 2012. The 2011 was collected with $\sqrt{s} = 7$ TeV and has an integrated luminosity of $\int L(t) dt = 4.75 fb^{-1}$, whilst the 2012 data was collected with $\sqrt{s} = 8$ TeV and has an integrated luminosity of $\int L(t) dt = 6.05 fb^{-1}$. Both data sets came from the egamma stream; this refers to the set of triggers used and each event has to contain electron or photon candidates. It is important to remember that the data set initially contains a large number of objects faking electron or photon signals.

3 The Analysis Procedure

The analysis was performed using Athena and the ZeeD program [5]. This is a program specifically designed for analysing the Z boson decay to an electron-positron pair. The ZeeD program analyses the preprocessed events and through a series of cuts selects those which are consistent with the Z boson electron decay channel. This occurs in a two stage process: first all the events are tested with a small set of crude cut and then the events which pass these are exposed to more stringent set of cuts. The purpose of the crude cuts is to quickly evaluate whether the event will be useful or not so that processing time is not wasted. The full list of the cuts used in this analysis is available in Table 1. The sample of events which pass the tight cuts is then used for further analysis.

3.1 The Tag and Probe Method

This analysis used the tag and probe method [6]; this application of the method involved strongly selection for Z bosons and then strongly selecting one of the decay products to be an electron (or positron); this electron is known as the "tag". As the Z boson decay must conserve charge and lepton number we know that the other particle must be an electron (or positron); this particle is called the "probe". The probe electron is then used to measure the efficiency of the cut where the efficiency of that cut is given by equation 1 where N^{Uncut} is the number of probes before the cut and N^{Cut} is the number after the uncut. Through selecting only probes within certain energy or pseudo-rapidity ranges it is possible to study how the efficiency varies as a function of these parameters.

Table 1: A table showing the selection cuts used

| ZeeD Selection Cuts | Description |
|----------------------------|--|
| ExistZ | A Z boson must be reconstructed in the event |
| PtMinBothElecZ | The e^\pm must have more than a certain transverse momentum |
| EtaMaxBothElecZ | The e^\pm pseudo-rapidity must be less than a certain limit |
| EtaCrackBothElecZ | The e^\pm must not lie in the calorimeter transition region |
| ZMassZ | The e^\pm pair's invariant mass must lie with a certain range |
| AuthorBothElecZ | Both the calorimeter and the trackers must be used in the reconstruction |
| IsEMTightPPBothElecZ | The e^\pm must pass a set of stringent identification cuts |
| ChargeBothElecOppositeZ | The e^\pm pair must have opposite charges |
| NTracksAtPrimVtx | There must be a minimum number of tracks from the primary vertex |
| OQMaps | The e^\pm cannot pass through malfunctioning detectors |
| TrigDefaultDiElecBothElecZ | The e^\pm must be matched to the trigger chains |
| MaxTwoGoodElec | No more than two good e^\pm candidates can be reconstructed |
| ZeeDCutLArEventVeto | The hadronic calorimeter must be functioning correctly |

$$\epsilon_{\text{Name of Cut}} = \frac{N^{\text{Cut}}}{N^{\text{Uncut}}} \quad (1)$$

Through a comparison between the efficiencies in the data and MC we can see how well our MC matches our data and correct the MC accordingly. To correct the MC we use a scale factor as defined in equation 2.

$$SF = \frac{\epsilon_{\text{Data}}}{\epsilon_{\text{MC}}} \quad (2)$$

3.2 Isolation Cuts

This study investigated the effect of two types of isolation: tracker isolation and calorimeter isolation. Isolation is a measure of the relative strength of the electron signal in the detector compared to the strength of the signals from other particles in a nearby region to the electron. It is an important parameter as it can be used to help differentiate between electrons produced directly from a Z boson and those produced in jets. The cut works by calculating the relative importance of the electron's transverse momentum or energy to the total transverse momentum or energy recorded by the detector in a cone about the electron's path. The cut eliminates events where there are large contributions to the cone which do not come from the electron. The cut is useful as electrons produced

straight from the Z boson are likely to be isolated and have no nearby high energy tracks. For electrons produced in jets this will not be the case and it is likely that they will be surrounded by other high energy particles and so hopefully will be removed by this cut.

There are a range of these cuts which work on the tracker and the calorimeter and have different cone sizes and/or different stringencies of cut. The isolation is measured within one of three possible size cones: 0.2, 0.3 or .4. The isolation cut is a dynamic cut and cuts data to achieve a desired efficiency and so does not cut at a fixed value. In our study we investigated four different predicted efficiencies 95%, 97%, 98%, 99%. The isolation cut also has built in corrections for transverse momentum leakage corrections and to correct for pile up (something that was investigated). Each cut is named with the following convention: firstly there is a number representing the preset efficiency, then there is a name stating whether it is a calorimeter based, Etcone, or a tracker based, Ptcone, cut and then finally there is a number giving the cone size. An example is 97Ptcone40; this is a tracker based cut with a preset efficiency of 97% and a cone size of .40.

3.3 Scale Factor dependencies

Through the measurement of the probe electron's properties it is possible to study the dependency of the efficiency (and thus the scale factors) on many parameters. Understanding the dependency of the scale factor on various properties is important as if strong dependencies exist the correction to the MC simulation must be applied as a differential to avoid inaccurately scaling the Monte Carlo. This study investigated the dependency on the transverse momentum (P_T), the pseudo-rapidity (η), mu (μ) and the number of primary vertices (NumVtx). Table 2 shows the range of the parameters probed. The pseudo-rapidity variable is only investigated in this small region as this is the only area where good tracking exists and the exclusion of $1.37 < |\eta| < 2.47$ arises as this is the transition region from the barrel to the end-cap calorimeters.

Table 2: A table showing the probed parameter ranges

| Parameter | Range |
|-----------|--|
| P_T | $> 20 \text{ GeV}$ |
| η | $0 < \eta < 1.37$ and $1.52 < \eta < 2.47$ |
| μ | $\mu > 0$ |
| NumVtx | NumVtx > 0 |

From 2011 to 2012 the instantaneous luminosity and the beam energy were increased;

one result of this is more pile-up. In an ideal situation the collider would collide one proton with one proton exactly every time; however, this is neither possible nor efficient. Instead the protons travel around the LHC in groups (known as bunches) and these bunches then collide. When they collide multiple proton-proton collisions occur and thus the detectors receive data from many collisions almost simultaneously, an effect known as pile-up.

Mu and NumVtx are measures of this pile up effect; mu is the mean number of interactions per crossing for each bunch and is given by $\mu = \frac{L_{Bunch} \times \sigma_{inel} \times n_{bunch}}{f_r}$ where L_{Bunch} is the instantaneous luminosity of the bunch, σ_{inel} is the inelastic cross section and f_r is the LHC revolution frequency; and NumVtx is the number of primary vertices measured by the detector. Graph 2 shows how the peak mu varies with time and it is easily seen that the pile up is significantly larger in 2012 than in 2011. It was thought that this increase in pile-up would result in reduced efficiencies particularly for the isolation cut and this was investigated in this study.

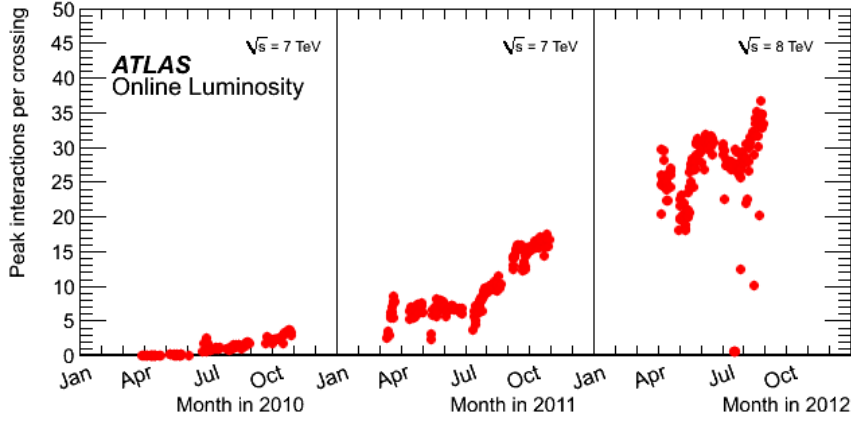


Figure 2: A graph showing how mu varies with time

4 Results and Analysis

4.1 Efficiency Cross Check

The first stage of the analysis was to check whether the isolation cuts were cutting to the correct efficiency, i.e. whether at 95% isolation cut did indeed have a 95% efficiency. Table 3 shows all the different isolation cuts that were investigated together with the efficiency that was measured when these cuts were applied to a 2011 Monte Carlo sample. As can be seen the isolation cuts all are in good agreement with the preset efficiency. The rest of the report will be focused on the 97Ptcone40, the 98Etcone20 and their combined

effect. This was done solely to allow for the discussion of a greater range of the isolation cut properties.

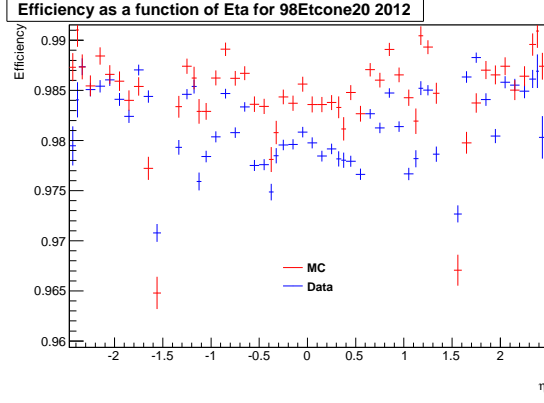
Table 3: A table showing the different Isolation cut and their measured efficiencies

| Isolation Cut Type | Efficiency (Fitted) |
|---------------------------|---------------------|
| 98Etcone20 and 97Ptcone40 | 0.955 |
| 98Etcone20 and 98Ptcone40 | 0.964 |
| 98Etcone20 and 99Ptcone40 | 0.972 |
| 98Etcone20 and 97Ptcone30 | 0.955 |
| 98Etcone20 and 99Ptcone30 | 0.973 |
| 98Etcone20 and 98Ptcone20 | 0.964 |
| 97Ptcone40 | 0.972 |
| 98Ptcone40 | 0.982 |
| 99Ptcone40 | 0.991 |
| 97Ptcone30 | 0.972 |
| 99Ptcone30 | 0.991 |
| 98Ptcone20 | 0.982 |
| 95Etcone20 | 0.952 |
| 98Etcone20 | 0.981 |
| 98Etcone30 | 0.981 |

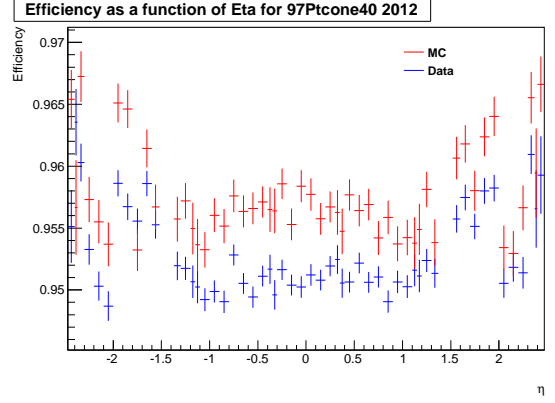
4.2 The pseudo-rapidity dependence of the efficiencies and scale factors

The next property that was investigated was the dependence of the efficiency on the pseudo-rapidity. This was achieved by binning the data into small pseudo-rapidity bins and then calculating the efficiency of the individual bins. The graphs 3a, 3b and 3c show the result of this operation for the three isolation cuts on the 2012 data set.

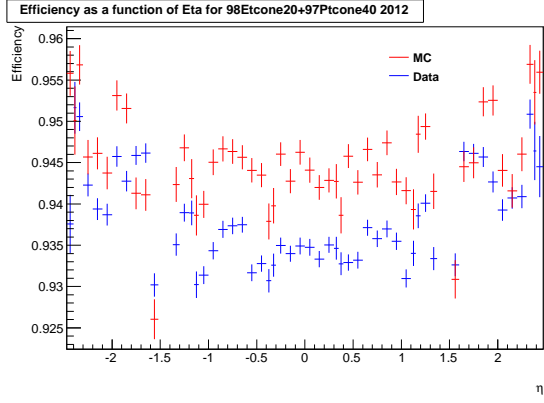
There are several interesting features shown in these graphs; the first is that there is a drop in the efficiency for $|\eta|$ near $\eta = 1.5$ in the calorimeter isolation. It is likely that this is an effect caused by the change from the central calorimeters to the end-cap calorimeters (an effect which is persistent despite the pseudo-rapidity cut). The next interesting effect is that for all the isolation cuts an increased efficiency is seen in the forward most regions. This is the opposite to what was expected, as the detectors in the end-caps are of worse granularity it was expected that we would observe a reduced efficiency. It is possible that this effect arises due to insufficient background suppression or due to an inaccurate calibration or reweighting.



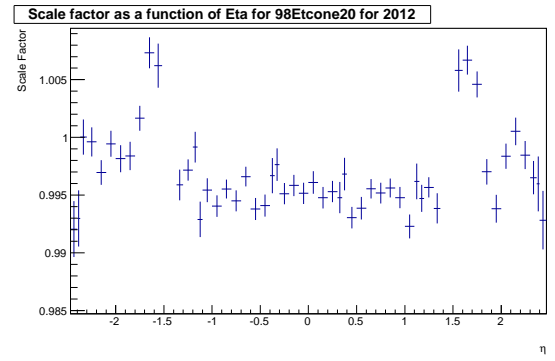
(a)



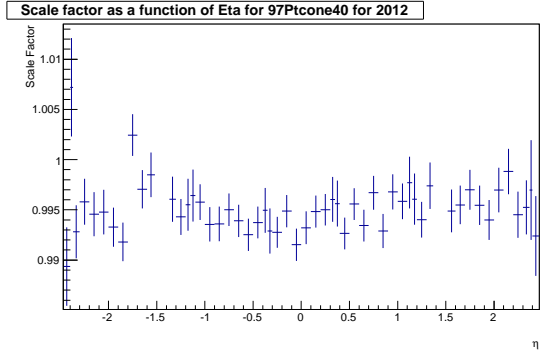
(b)



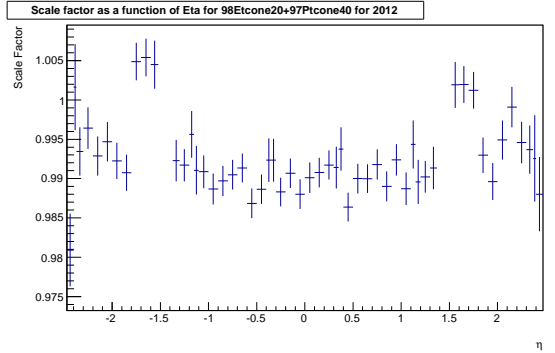
(c)



(d)



(e)



(f)

Figure 3: The scale factor and efficiency pseudo-rapidity distributions for the three different isolation cuts

Next it was instructive to view the pseudo-rapidity dependence of the scale factors. This is done in graphs 3d, 3e and 3f. The scale factors are close to one which shows that the Monte Carlo is in quite good agreement with the measured data for 2012. The fact that they are less than one shows the Monte Carlo simulation is more efficient than the data.

The 97Ptcone40 is almost independent of pseudo-rapidity whereas the 98Etcone20 shows a slight increase with increasing pseudo-rapidity .

It was important to investigate whether the analysis was consistent between 2011 and 2012. Graph 4 shows how the scale factor for the combined 98Etcone20+97Ptcone40 varies as a function of pseudo-rapidity for both 2011 and 2012. It can be seen that they have similar scale factors for all the pseudo-rapidity bins and so both show the same features. The 2011 scale factors are slightly larger for small pseudo-rapidity values resulting in a distribution which, excluding the calorimeter transition spikes, is almost independent of pseudo-rapidity .

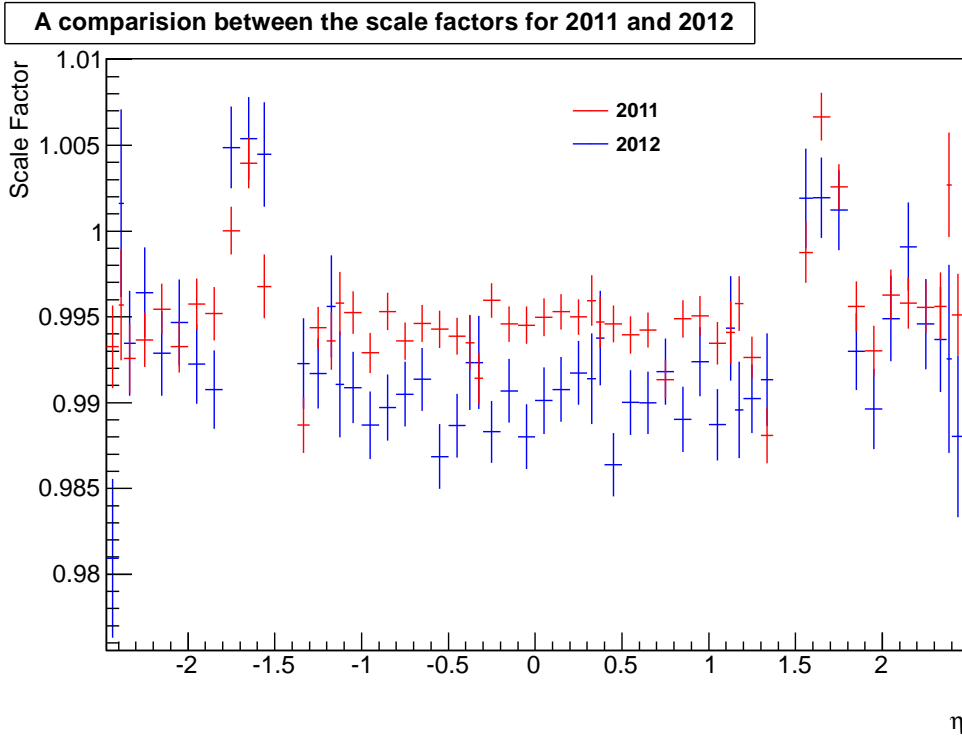


Figure 4: A comparison between the scale factor distributions in pseudo-rapidity for 2011 and 2012

4.3 Systematic Errors from the Mass selection

In addition to understanding the statistical errors associated with our scale factors, it is important to understand the systematic errors. One of the largest systematic errors introduced by this analysis method was from the choice of the electron-positron invariant mass range (85 – 95 GeV). This mass range was chosen to ensure that only background free Z boson candidates were selected; however, this choice of range will have introduced

a systematic error.

To estimate the magnitude of the systematic error that was introduced, the analysis was repeated by using different mass ranges and then these were compared with the original range. In this study two alternative mass ranges were investigated: $85 - 95$ GeV and $75 - 105$. These mass ranges were chosen to be almost symmetric about the Z boson peak so that there is no confusion between the effect of systematic errors and any mass dependent effects.

In graphs 5a and 5b the difference between the scale factors from these altered mass ranges and the original mass range are plotted as a function of NumVtx. It can be seen that the resulting differences, in both cases, are less than 0.2% of the original scale factors and thus there only a small systematic error could have been introduced. The differences are almost completely independent of pile-up (for the strength of pile-up observed in 2012) and thus the systematic errors must also be independent of pile up.

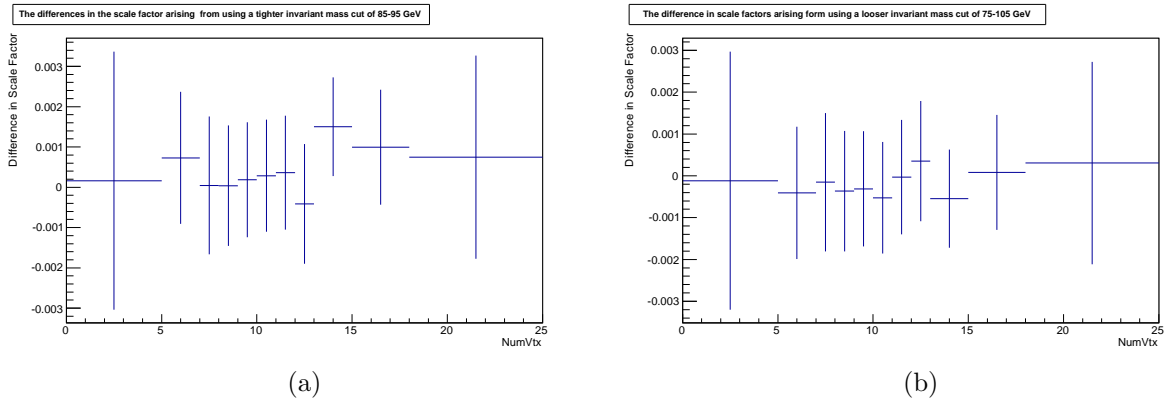


Figure 5: The scale factor differences associated with using different sized symmetric mass ranges for the 2012 data set and the 97Ptcone40+98Etcone20 cut

4.4 Mass Dependence

It was interesting to investigate whether the scale factors exhibited any mass dependence; to do this the analysis was rerun using invariant mass ranges which were not symmetric about the Z boson mass peak. In this analysis two invariant mass cuts were investigated: the first was below the mass peak and covered the range $75 - 90$ GeV and the other bin was approximately above the peak and covered the range $90 - 105$ GeV. By comparing the scale factors and efficiencies measured in these bins it is possible to test whether there is any mass dependence.

Graphs 6a and 6b show the deviation in the efficiencies, as a function of the number of primary vertices (NumVtx), for the asymmetric mass ranges from the standard mass

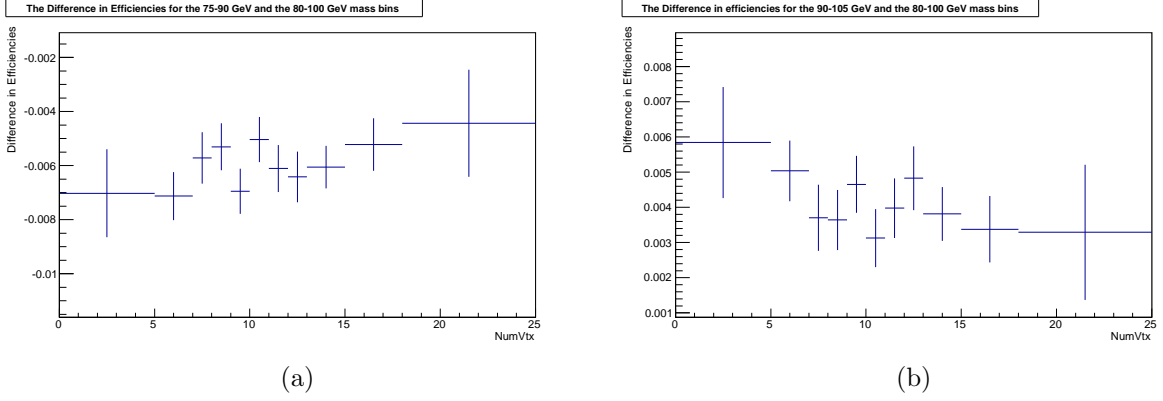


Figure 6: The efficiency differences associated with using mass ranges which are asymmetric about the Z boson mass peak in the 97Ptcone40+98Etcone20 cut

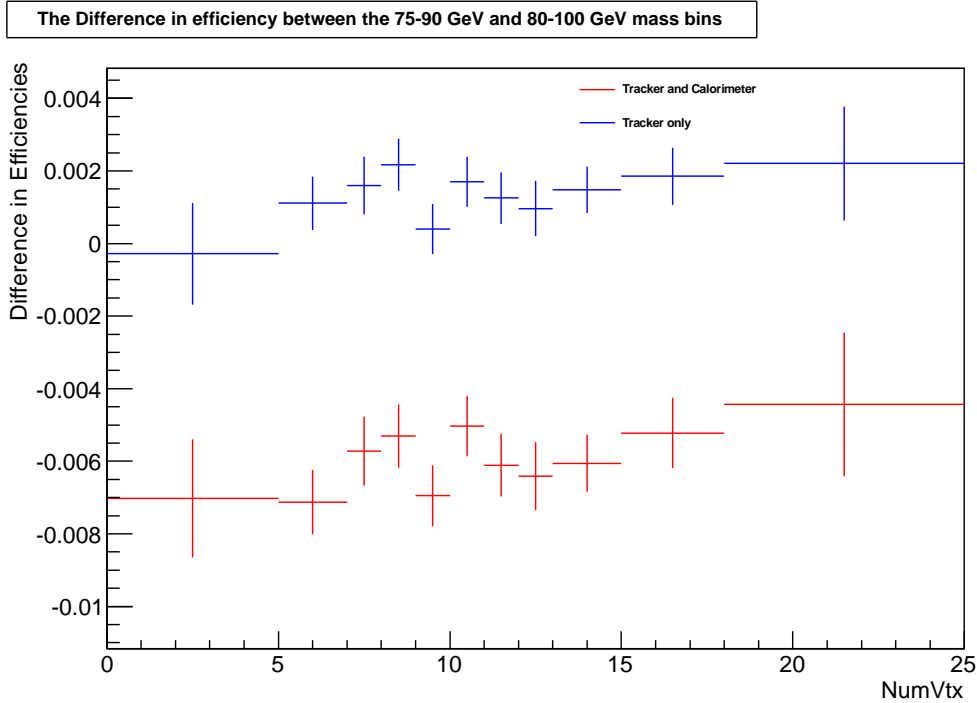


Figure 7: A comparison between the 97Ptcone40 isolation cut efficiency and the 97Ptcone40+98Etcone20 cut efficiency for the 2012 data

range of 80 – 100 GeV. These graphs are for the 97Ptcone40+98Etcone20 cut using 2012 data set. It is interesting to observe that the mass range below the peak has scale factors which are significantly less than the symmetric range; this is a property which is shown for all of the NumVtx bins. The mass range above the peak shows a slight increase in the efficiencies which shows a weak trend with the NumVtx.

One possible explanation for this mass dependence comes from bremsstrahlung radiation. There are two types of bremsstrahlung: internal and external. Internal bremsstrahlung refers to non virtual photons emitted from the other quarks and gluons involved in the interaction. External bremsstrahlung is radiation emitted when the electrons interact with the material in the detector and radiate. Bremsstrahlung radiation is often present in an event with a significant proportion of the photons lying within the isolation cone and thus, if their energy is sufficiently large, they will result in the electron or positron failing the isolation cut. This effect is most prominent in the lower mass range as when the electrons radiate they lose energy; the result of this is that the measured invariant mass of the electron positron pair is less. Thus the events in which large amounts of radiation are produced are more likely to be found in the lower mass range and thus the lower mass range will have more events failing the isolation cut.

There was a method to test this theory; photons are not detected by the trackers and so this decrease in efficiency should not be seen in the 97Ptcone40 (the tracker based) isolation cut. Graph 7 shows the difference in the lower mass range and the standard mass range efficiencies for both the tracker isolation cut (97Ptcone40) and the combined tracker and calorimeter isolation cut (97Ptcone40+98Etcone20) for the 2012 data. It can be seen that the tracker isolation cut does not show the same decreased efficiency that is seen in the combined cut, thus supporting the theory.

4.5 The Dependence on the Number of Primary Vertices

As pile up increases the efficiency of the isolation cut would ordinarily decrease, however the isolation cut has an inbuilt scaling which attempts to correct for the increased pile up. Graphs 8a and 8b show how the scale factors for the 98Etcone20 cut and 97Ptcone40 cut in 2012 vary as a function of the number of primary vertices. Despite the correction in the isolation cuts, both still show a dependence on the number of primary vertices.

This dependency was then investigated as a function of pseudo-rapidity; this study was performed as it was thought that there would be stronger pile up dependency in the forward most pseudo-rapidity bins as these were most likely to get swamped by soft collisions. To do this the events were put into one of five different pseudo-rapidity bins: $0 < |\eta| < 0.4$, $0.4 < |\eta| < 0.8$, $0.8 < |\eta| < 1.37$, $1.37 < |\eta| < 2.0$ and $2.0 < |\eta| < 2.47$. For each pseudo-rapidity bin the efficiency was investigated as a function of the number of primary vertices. Graph 9 shows the results for the $0.8 < |\eta| < 1.37$ pseudo-rapidity bin for 2012 in the with the tracker based cut (97Ptcone40). Each of these graphs were then fitted with a straight line and the gradient of this was plotted as function of the modulus of the pseudo-rapidity.

Graphs 10c, 10b and 10a show the fitted gradient as a function of the modulus of the pseudo-rapidity for the 2012 data. As can be seen in graph 10b the 97Ptcone40 isolation

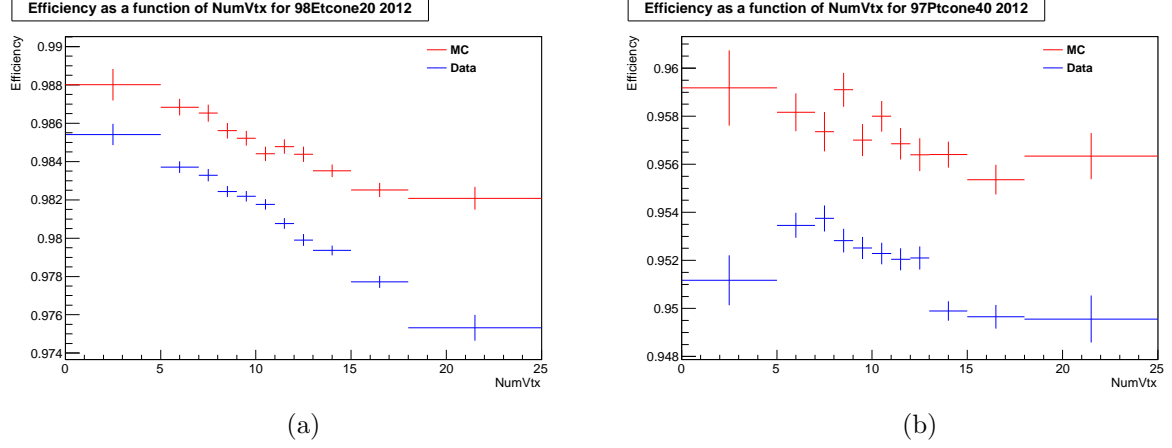


Figure 8: The scale factors' dependency upon the number of primary vertices for the 97Ptcone40 and 98Etcone20 cuts in 2012

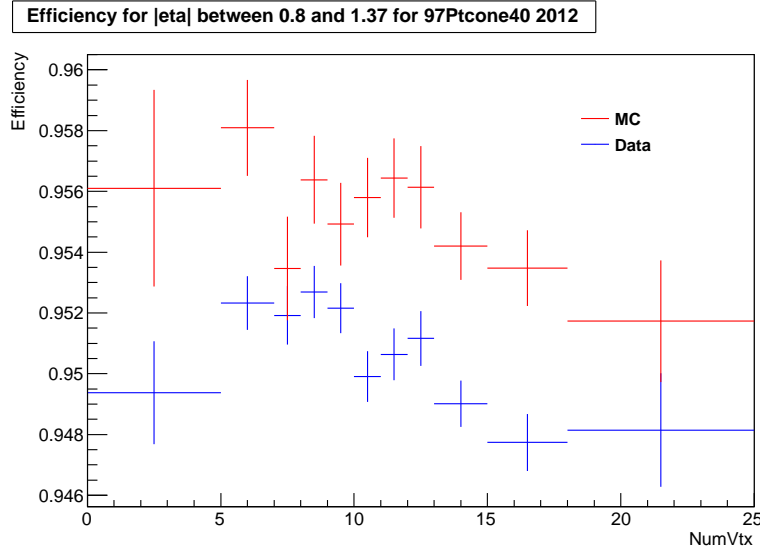
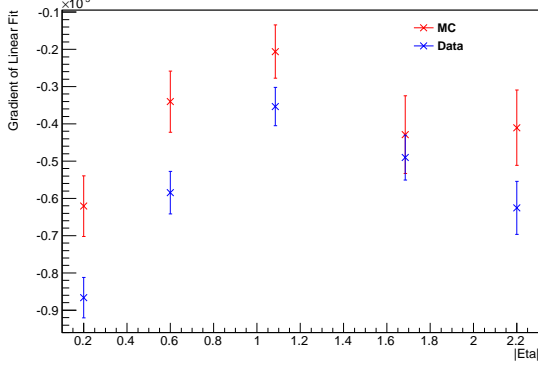


Figure 9: A graph showing how the efficiency varies as a function of the number of primary vertices for events with pseudo rapidities with a magnitude between .8 and 1.37 for the 97Ptcone40 isolation cut.

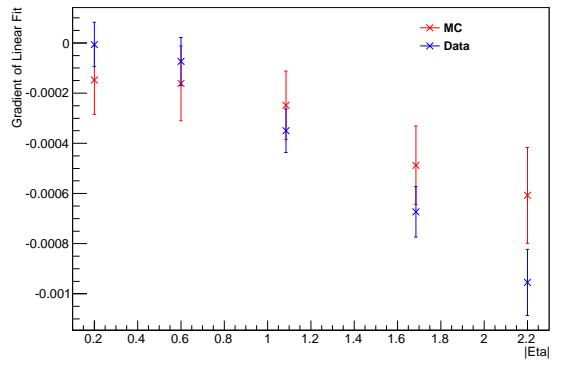
cut shows this expected trend; however, this trend is not observed in the 98Etcone20 cut as is shown in graph 10a. The exact reason as to why this is not observed is not yet known; it is thought that it may occur due to a difference in calorimeter granularity. The calorimeter within the region $|\eta| < 0.8$ is of a different resolution to the rest of the barrel and it was thought that some inaccurate calibration may have caused the observed effect. As the $0.4 < |\eta| < 0.8$ shows a weaker dependence on the number of vertices than the $|\eta| < 0.4$ bin it is unlikely that this is the full reason behind the

The variation of the gradient of a linear fit for each eta bin for 98Etcone20 2012



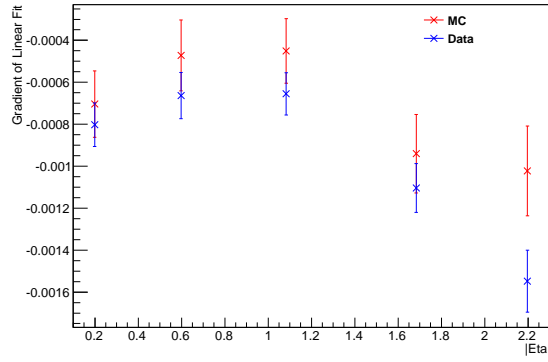
(a)

The variation of the gradient of a linear fit for each eta bin for 97Ptcone40 2012



(b)

The variation of the gradient of a linear fit for each eta bin for 98Etcone20+97Ptcone40 2012



(c)

Figure 10: The variation in the efficiencies dependence on the number of primary vertices as both the pseudo-rapidity and the type of isolation cut are changed.

difference; thus further study into this effect is required.

4.6 Mu Dependence

The Mu dependence of the efficiency was also investigated; it was expected that the mu dependence would be similar to the NumVtx dependence as they are both measures of pile up. Graphs 11a and 11b show how the efficiencies for the 97Ptcone40 and 98Etcone20 vary as a function of mu for the 2012 data set. It is interesting to see that the mu dependence is not the same as the NumVtx dependence. Despite measuring the same effect, the mu and NumVtx variables are different; the mu variable is a measure of the average number of interactions and comes from the accelerator, whereas the NumVtx variable is an exact measure of the number of primary vertices as measured by the detector. It is thought that this difference in the definitions results in the different behaviour

observed in the efficiencies.

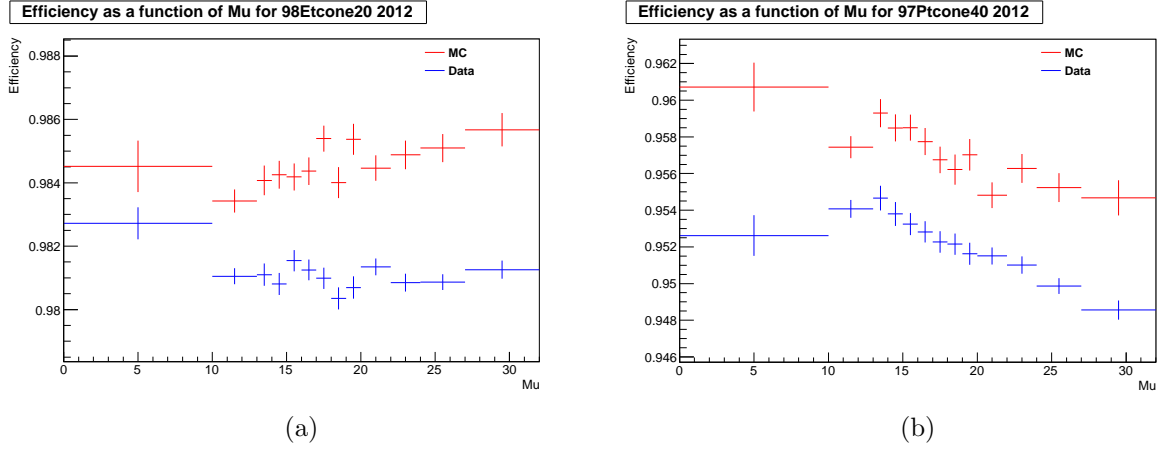


Figure 11: The efficiency's dependency upon μ for the 97Ptcone40 and the 98Etcone20 cuts in 2012

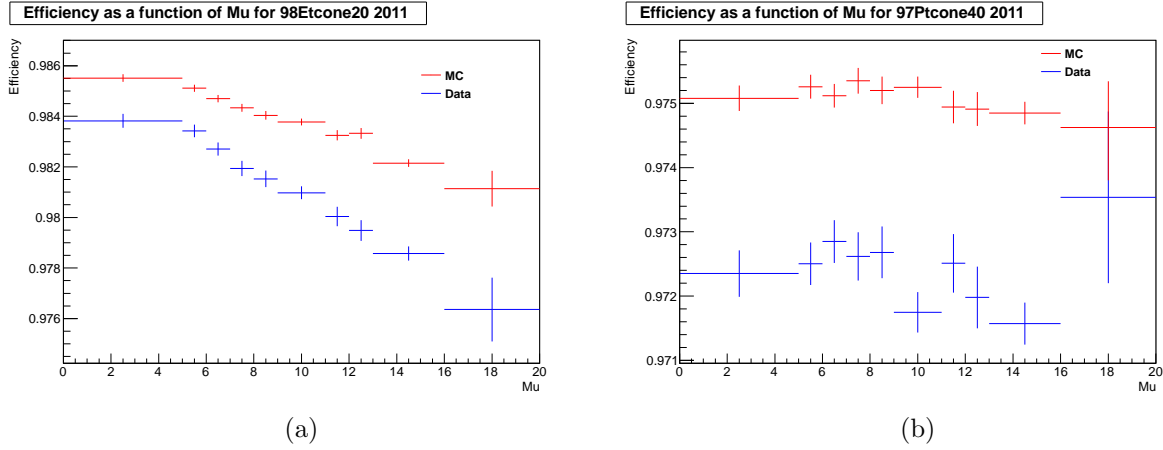


Figure 12: The efficiency's dependency upon μ for the 97Ptcone40 and the 98Etcone20 cuts in 2011

It was also of interest to make a comparison between the 2011 and 2012 data sets. Graphs 12a and 12b show how the efficiencies for the 97Ptcone40 and 98Etcone20 cuts vary as a function of μ for the 2011 data set. A very interesting discrepancy was observed here; the efficiency of the 2012 98Etcone20 cut shows effectively no dependence on μ . This is in contrast with the 2011 data, where the 98Etcone20 cut efficiency decreases with increasing μ .

One possible explanation for this difference is that it is a result of the change in center of mass energy, from $\sqrt{s} = 7$ TeV to $\sqrt{s} = 8$ TeV. This change results in an altered relation between mu and the NumVtx variables changed. Due to the isolation's scaling as a function of the NumVtx variable, both years will exhibit similar dependencies on that variable, but this altered mu and NumVtx relation could result in different mu dependence. Another possible explanation is that the offset correction for the average pile-up generated energy could be different between the two years. The graph 13 shows the distribution of the energy measured in a .20 cone in the calorimeter divided by the electron's transverse momentum for 2011 and 2012. The distributions peak at different points and have different widths and this could be the source of the discrepancy, however further study is required to test this idea.

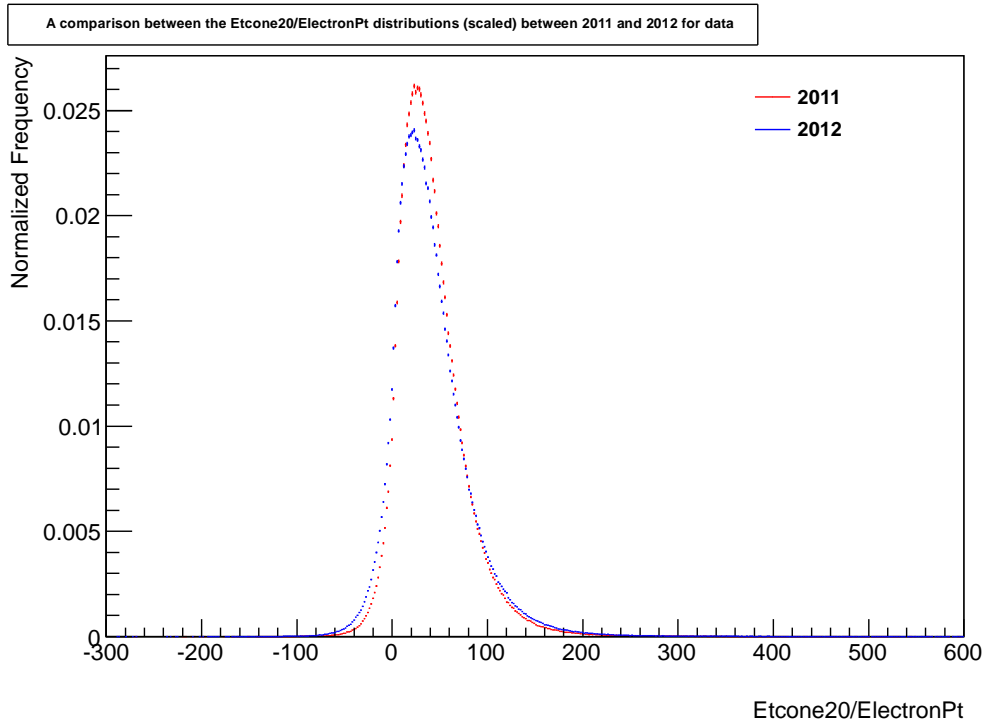


Figure 13: A graph showing a comparison between the normalised Etcone20/Electron transverse momentum distributions of 2011 and 2012

5 Conclusion

The tag and probe method was implemented and used to study the efficiency of several isolation cut variants used in the analysis of the decay of the Z boson to an electron-positron pair. The analysis was performed upon data collected by the ATLAS experiment at the Large Hadron Collider. Two data sets were investigated: the full 2011 data set

which has an integrated luminosity of $\int L(t) dt = 4.75fb^{-1}$ and a center of mass energy of $\sqrt{s} = 7$, and periods A and B from 2012 which has $\int L(t) dt = 6.05fb^{-1}$ and $\sqrt{s} = 7$. This data was compared with Monte Carlo samples generated by the PYTHIA and POWHEG programs.

The isolation cut efficiency of the data was found to be in good agreement with the Monte Carlo samples, as is seen with scale factors very close to one. The efficiency was found to be dependent upon the electrons' pseudo-rapidity, the number of primary vertices and mu (though the mu dependency is not universal). The pseudo-rapidity and the number of primary vertices dependencies were not as had been expected, but it was postulated these effects arose due to inaccuracies in calibration and reweighting.

Though comparisons between the two years it was found that the analysis works well for both years, with generally good agreement. A discrepancy in the mu dependence of the efficiency between the two years was observed. This was thought to have been caused either by differing offset set corrections for the average pile-up generated energy between the two years or because of the mu's dependency on the centre of mass energy.

The scale factors and efficiencies were found to be dependent upon the centre of mass energy of the electron-positron pair, with lower mass pairs having lower isolation cut efficiencies. This effect is thought to be a result of bremsstrahlung radiation and this view is supported by the fact the mass dependence was not observed in the 97Ptcone40 isolation cut efficiency. The systematic error resulting from the constraint on the center of mass energy of the electron-positron was calculated and found to be less than 0.2% and also was found to be independent of the number of primary vertices.

There is still a significant amount of further study required as there are still several unexplained effects observed in the data. It would be useful to investigate how significant the effect of the background is and also to analyse the other contributions to the scale factor's systematic errors.

References

- [1] Measurement of the inclusive W^\pm and Z/γ^* cross sections in the electron and muon decay channels in pp collisions at $\sqrt{s} = 7$ TeV with the ATLAS detector *The ATLAS Collaboration*
- [2] The ATLAS Experiment at the CERN Large Hadron Collider *The ATLAS Collaboration*
- [3] PYTHIA 6.4 Physics and Manual *Torbjorn Sjostrand, Stephen Mrenna and Peter Skands*
- [4] Matching NLO QCD computations with Parton Shower simulations: the POWHEG method *Stefano Frixione, Paolo Nason and Carlo Oleari*
- [5] The ZeeD program <https://svnsrv.desy.de/desy/Zeed/trunk> *The ZeeD group, DESY*
- [6] Electron performance measurements with the ATLAS detector using the 2010 LHC proton-proton collision data *The ATLAS Collaboration*